Timescale separation in the solar wind-magnetosphere coupling during St. Patrick's Day storms in 2013 and 2015

Alberti, T.; Consolini, G.; Lepreti, F.; Laurenza, M.; Vecchio, A.; Carbone, V.

DOI:
10.1002/2016JA023175

AGU PUBLICATIONS

JGR

Journal of Geophysical Research: Space Physics

RESEARCH ARTICLE
10.1002/2016JA023175

Special Section:
Geospace system responses to the St. Patrick's Day storms in 2013 and 2015

Timescale separation in the solar wind-magnetosphere coupling during St. Patrick's Day storms in 2013 and 2015

T. Alberti[1], G. Consolini[2], F. Lepreti[1], M. Laurenza[2], A. Vecchio[3], and V. Carbone[1]

[1]Department of Physics, University of Calabria, Rende, Italy, [2]INAF-Istituto di Astrofisica e Planetologia Spaziali, Rome, Italy, [3]LESIA-Observatoire de Paris, Meudon, France

Key Points:
- Novel analysis approaches clearly indicate the existence of a relevant timescale separation in the solar wind-magnetosphere coupling
- Short-timescales (200 min) fluctuations, triggered by changes of the interplanetary conditions, are mainly related to internal processes
- The magnetospheric dynamics at timescales longer than 200 min resembles the changes observed in the solar wind/IMF features

Correspondence to:
T. Alberti,
tommaso.alberti@unical.it

Citation:
Alberti, T., G. Consolini, F. Lepreti, M. Laurenza, A. Vecchio, and V. Carbone (2017), Timescale separation in the solar wind-magnetosphere coupling during St. Patrick's Day storms in 2013 and 2015, *J. Geophys. Res. Space Physics*, *122*, 4266–4283, doi:10.1002/2016JA023175.

Received 15 JUL 2016
Accepted 15 MAR 2017
Accepted article online 21 MAR 2017
Published online 19 APR 2017

Abstract In this work, we present a case study of the relevant timescales responsible for coupling between the changes of the solar wind and interplanetary magnetic field (IMF) conditions and the magnetospheric dynamics during the St. Patrick's Day Geomagnetic Storms in 2013 and 2015. We investigate the behavior of the interplanetary magnetic field (IMF) component B_z, the Perreault-Akasofu coupling function and the *AE*, *AL*, *AU*, *SYM-H*, and *ASY-H* geomagnetic indices at different timescales by using the empirical mode decomposition (EMD) method and the delayed mutual information (DMI). The EMD, indeed, allows to extract the intrinsic oscillations (modes) present into the different data sets, while the DMI, which provides a measure of the total amount of the linear and nonlinear shared information (correlation degree), allows to investigate the relevance of the different timescales in the solar wind-magnetosphere coupling. The results clearly indicate the existence of a relevant timescale separation in the solar wind-magnetosphere coupling. Indeed, while fluctuations at long timescales ($\tau > 200$ min) show a large degree of correlation between solar wind parameters and magnetospheric dynamics proxies, at short timescales ($\tau < 200$ min) this direct link is missing. This result suggests that fluctuations at timescales lower than 200 min, although triggered by changes of the interplanetary conditions, are mainly dominated by internal processes and are not directly driven by solar wind/IMF. Conversely, the magnetospheric dynamics in response to the solar wind/IMF driver at timescales longer than 200 min resembles the changes observed in the solar wind/IMF features. Finally, these results can be useful for Space Weather forecasting.

1. Introduction

The Earth's magnetospheric dynamics in response to changes of the solar wind (SW) and interplanetary magnetic field (IMF) conditions during magnetic storms and substorms is the result of both externally driven and internal processes that can be investigated via a set of geomagnetic indices. These geomagnetic indices monitor the changes of some of the most important current systems. In particular, the variations of the auroral electrojet indices (*AE*, *AU*, *AL*, and *AO*) and the low-latitude geomagnetic ones (*Dst*, *SYM-H*, and *ASY-H*) are associated with the changes of the high-latitude ionospheric auroral electrojets and the equatorial ring current during geomagnetic substorms and storms, respectively. The changes of these current systems result from the magnetospheric configuration and dynamics, being affected by the energy transfer from the solar wind to different regions of the magnetosphere through electromagnetic processes [*Perreault and Akasofu*, 1978]. This interaction involves a considerable energy transfer by the solar wind, which manifests itself in several fast phenomena occurring in the magnetosphere such as auroral displays, magnetic substorms, and storms [*Tsurutani et al.*, 2015].

As a consequence of the solar wind-magnetosphere interaction, these indices display both regular and irregular variations/fluctuations on a very wide interval of timescales [*Merrill et al.*, 1996; *De Michelis et al.*, 2015], ranging from a few tens of minutes up 200 min. The observed multiscale variations/fluctuations have been shown to be also due to a complex and nonlinear dynamics of the Earth's magnetosphere [*Tsurutani et al.*, 1990; *Sharma*, 1995; *Vassiliadis*, 2006; *Consolini and De Michelis*, 2014]. Indeed, in the last two decades many studies evidenced how the multiscale character of the fluctuations/variations of geomagnetic indices is associated with fractal/multifractal scaling features of the corresponding time series [*Consolini et al.*, 1996; *Consolini*, 1997; *Uritsky and Pudovkin*, 1998; *Kovacs et al.*, 2001; *Wanliss*, 2005; *Consolini and De Michelis*, 2011] and power law distributions of the associated energy dissipation events [*Consolini*, 1997, 2002; *Wanliss and Uritsky*, 2010].

All these features have been interpreted as evidences of a far-from-equilibrium nonlinear dynamics near a critical state [see, e.g., *Klimas et al.*, 1996; *Sitnov et al.*, 2001; *Consolini and Chang*, 2001; *Consolini*, 2002; *Uritsky et al.*, 2002; *Consolini et al.*, 2008]. An important consequence of this nonlinear and near-critical-state dynamics of the Earth's magnetosphere is that there is not a one-to-one correspondence between the SW/IMF condition changes and those of the magnetospheric current systems as monitored by geomagnetic indices [*Sitnov et al.*, 2001; *Consolini*, 2002]. In other words, the dynamics of the magnetospheric currents and of the overall magnetosphere, although triggered by the variation of the interplanetary conditions, is strongly affected by the internal conditions. This is exactly what has been understood since the early works on the nonlinear and pseudochaotic dynamics of the Earth's magnetosphere [see, e.g., *Tsurutani et al.*, 1990; *Klimas et al.*, 1996].

A relevant issue in the study of the solar wind-magnetosphere coupling is related to the different timescales involved in the internal and externally driven processes. For instance, geomagnetic substorms are mainly the result of two different phenomena: the increase of plasma convection and fast energy relaxations occurring in the near-Earth tail central plasma sheet (CPS) [*Rostoker et al.*, 1987; *Kamide and Kokubun*, 1996; *Consolini and De Michelis*, 2005]. These two phenomena, which are connected to the direct-driven and loading-unloading processes, are characterized by different timescales. In particular, while loading-unloading processes generally occur on short timescale ($\tau < 100$ min) and manifest themselves in terms of coherent intermittent activity bursts, the externally direct-driven ones take place on longer timescales [*Kamide and Kokubun*, 1996; *Consolini and De Michelis*, 2005].

The identification of the timescales directly connected to the external solar wind variability and to the internal magnetospheric dynamics is also a relevant issue in the framework of Space Weather studies. Indeed, this information is of fundamental importance to know to what extent we can forecast the magnetospheric dynamics starting from the measurement of the solar wind conditions. Attempts to forecast high-latitude geomagnetic disturbances as monitored by auroral electrojet indices (such as, *AE* index) via artificial neural networks have clearly shown how *AE* variations on timescales shorter than 1 h, cannot be correctly forecasted from IMF and solar wind plasma parameters only [see, e.g., *Pallocchia et al.*, 2007]. These studies suggest that fluctuations on timescale shorter than 1 h are essentially not coupled to solar wind variations but result from internal magnetospheric processes only.

In this work, we present a detailed study of the timescale coupling between SW/IMF condition changes, and the magnetospheric response in the course of the two St. Patrick's Day geomagnetic storms occurred in 2013 and 2015. To investigate the range of the coupled timescales, we use the empirical mode decomposition (EMD), which is particularly suitable for the analysis of nonlinear and nonstationary time series [*Huang et al.*, 1998], and the delayed mutual information (DMI), which is capable of providing a measure of the total linear and nonlinear correlation in terms of shared information.

2. Data and Methods

2.1. Data Sets and Geospace Conditions

We focus our analysis of relevant timescales involved into the solar wind-magnetosphere coupling considering two periods of 21 days from 10 to 30 of March 2013 and March 2015. These time intervals, which refer to the maximum phase (2013) of the Solar Cycle no. 24 (maximum sunspot number was observed in April 2014) and to the descending (2015) one, comprise both periods of low geomagnetic activity and the famous St. Patrick's Day geomagnetic storms. In particular, during the considered period in 2013, a halo coronal mass ejection (CME) was emitted on 15 March at 07:12, associated with an M1-flare located at N11E12 in the Active Region (AR) NOAA 1692. The CME had a linear speed of 1063 km/s and hit the Earth's magnetosphere at 06:00 UT on 17 March 2013 (storm sudden commencement, SSC), with the speed of the solar wind jumping from about 400 km/s to 750 km/s. Moreover, the CME's magnetic field was quite strong and oriented southward. The impact produced first a compression of the Earth's magnetosphere (solar wind pressure P_{SW} rose of a factor ~10) and, consequently to the southward orientation of the IMF B_z component, sparked a moderately strong ($Kp = 6$) geomagnetic storm.

In the same day of 2015, an asymmetric partial halo CME was observed at 01:48, having a linear speed of 719 km/s, and it was associated with a long duration C9.1 flare (location S22W25 in AR NOAA 2297). A shock in the solar wind parameters was observed by the ACE satellite shortly after 04:00 UT on 17 March, the solar wind speed jumping from 400 km/s to slightly above 500 km/s, then gradually increasing to a maximum of nearly 700 km/s over the next few hours. Except for a brief interruption between 09:00 and 11:00 UT,

the vertical component of the interplanetary magnetic field was consistently southward at about −20 nT from around 05:00 UT till 23:00 UT. First, the CME impact compressed the Earth's magnetosphere consequently to an increase of the flow pressure of a factor ∼3 ($p_{SW} \sim 15-20$ nPa) and, later, due to a southward turning of the IMF B_z component occurred at ∼06:00 UT, a relatively mild G1-class ($Kp = 5$) geomagnetic storm started. Since then, however, the storm has intensified to G4-class ($Kp = 8$), ranking it as the strongest geomagnetic storm of the current solar cycle (see http://swpc.noaa.gov/).

In this study, we use solar wind time series obtained from Advanced Composition Explorer (ACE) spacecraft (http://cdaweb.gsfc.nasa.gov), located at the Lagrangian point L1. In particular, we use data related to the three components (B_x, B_y, and B_z) of the interplanetary magnetic field (IMF) in GSM coordinates and the solar wind plasma bulk speed. In this way, we construct the Perrault-Akasofu coupling function ϵ which is defined as [*Perreault and Akasofu*, 1978]

$$\epsilon = \frac{4\pi}{\mu_0} l_0^2 v B^2 \sin^4(\theta_c/2) \quad [\mathrm{GW}] \tag{1}$$

where $\mu_0 = 4\pi \times 10^{-7}$ N/A^2 is the permeability of free space, $l_0 = 7\ R_E$ is the stand-off distance of the nose of the magnetosphere (also known as "effective cross-sectional area," "dayside magnetopause scale length," or simply seen as an empirical determined scale factor [*Perreault and Akasofu*, 1978; *Kan and Lee*, 1979; *Akasofu*, 1983; *Finch and Lockwood*, 2007]), v is the solar wind speed (in km/s), B is the magnitude of the solar wind magnetic field (in nT), and θ_c is the clock angle defined as

$$\theta_c = \begin{cases} \tan^{-1}\left(\left|\frac{B_y}{B_z}\right|\right), & \text{if } B_z > 0 \\ \pi - \tan^{-1}\left(\left|\frac{By}{Bz}\right|\right), & \text{if } B_z < 0. \end{cases}$$

Moreover, we analyze geomagnetic time series of the low-latitude *SYM-H* and *ASY-H* indices and the auroral electrojet indices, *AE*, *AU*, and *AL*, retrieved at OMNI website (http://omniweb.gsfc.nasa.gov). All the considered geomagnetic time indices have a 1 min time resolution. The *SYM-H* (a 1 min version of the well-known *Dst* index) and *ASY-H* indices, being derived from a network of near-equatorial geomagnetic observatories, allows us to get an estimate of the ring current dynamics and of the asymmetric low-latitude disturbance (partial ring current), respectively, in the course of a storm [*Sugiura and Poros*, 1971; *Kawasaki and Akasofu*, 1971; *Crooker and Siscoe*, 1971; *Crooker*, 1972; *Clauer and McPherron*, 1980; *Clauer et al.*, 1983]. On the other hand, the auroral electroject (*AE*, *AU*, and *AL*) indices (with 1 min resolution), derived from variations of the horizontal component (H) of the geomagnetic field at selected observatories along the auroral zone in the Northern Hemisphere [*Davies and Sugiura*, 1966], provide an estimation of the intensity of the electrojet currents in the auroral ionosphere and of the energy deposition in those regions [*Ahn et al.*, 1983]. In particular, *AE* index represents the overall activity of the auroral electrojets, while the *AU* and *AL* indices quantify the current intensity variations of the eastward and westward auroral electrojets, which are mainly related to the tail activity during magnetic storms and substorms.

Figure 1 shows the time series of the considered quantities (*SYM-H*, IMF-B_z, ϵ, *ASY-H*, *AE*, *AU*, and *AL*) for the two selected periods relative to the 2013 and 2015 St. Patrick's Day storms.

2.2. The Empirical Mode Decomposition (EMD) Method

The standard approach to identify the relevant timescales in a time series is based on Fourier analysis. Although this method is powerful in the case of stationary signals, it can produce fake results when it is applied to nonstationary time series. An alternative method to unveil the characteristic timescales of nonstationary signals is the empirical mode decomposition (EMD) technique, introduced by *Huang et al.* [1998] [see also *Wu and Huang*, 2004], as a preconditioning method for the application of the Hilbert transform. EMD is an adaptive method based on the local characteristics of the data, useful to analyze natural signals [*Vecchio et al.*, 2010a, 2010b, 2012a; *Alberti et al.*, 2014; *Vecchio et al.*, 2017], also including geomagnetic time series [*De Michelis et al.*, 2012; *De Michelis and Consolini*, 2015]. Particularly, the EMD does not require to have any "a priori" assumption on the functional form of the basis of the decomposition. This allows us to carry out local nonstationary and nonlinear features from each time series which are usually far from the decomposition properties obtained with fixed eigenfunctions. Here we use the same approach as proposed by *Huang et al.* [1998], with similar stopping criterion (i.e., the Cauchy convergence test with $\sigma = 0.3$), as previously used in other works [*Alberti et al.*, 2014, 2016] in which more details about the EMD procedure can be found. In what follows we provide a brief description of the method.

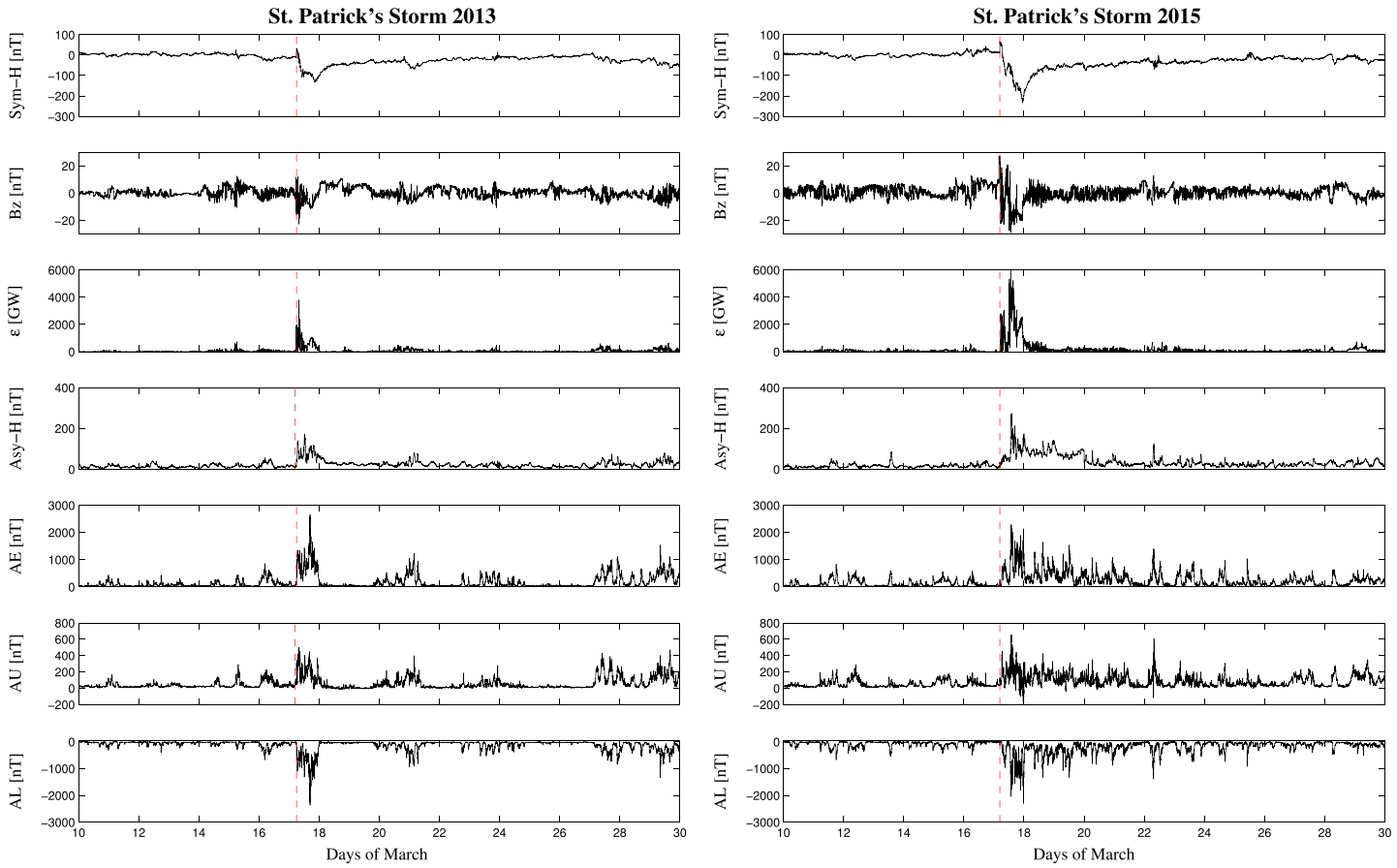

Figure 1. Time behavior of the solar wind parameters and the geomagnetic indices for both Storm time periods. The red dashed line identifies the SSC time.

A given time series $X(t)$ is decomposed into a set of N empirical modes $C_n(t)$, called intrinsic mode functions (IMFs) and ordered by increasing characteristic timescale, plus a residue $r(t)$. The decomposition reads

$$X(t) = \sum_{n=1}^{N} C_n(t) + r(t) \tag{2}$$

where each IMF is characterized by a time-dependent amplitude and phase ($C_n(t) = A_n(t)\sin(\phi_n(t))$, where $A_n(t)$ and $\phi_n(t)$ are the time-dependent amplitude and phase, respectively), and it is directly obtained from the time series with no a priori assumptions, regarding their nature, via an iterative procedure. Each IMF represents a local oscillatory component and the whole set of the IMFs becomes the basis of the decomposition (see *Huang et al.* [1998], *De Michelis et al.* [2012], and *Alberti et al.* [2014] for more details).

An example of the results of EMD analysis is shown in Figures 2 and 3 for the IMFs obtained using the *SYM-H* and *AE* indices for both periods. A set of $n = 15$ (14) and $n = 16$ (15) modes are extracted for the March 2013 (2015) time periods from *SYM-H* and *AE* indices, respectively, with characteristic timescales ranging from $\tau = 4$ min to $\tau \sim 10^4$ min. A similar number (14–17) of IMFs is found for the other parameters (B_z, ϵ, *ASY-H*, *AU*, and *AL*) in both selected time intervals.

To characterize the typical timescale associated with every IMFs, different methods can be used, from spectral method, based on the Fourier analysis of each IMFs, to autocorrelation-based methods and Max-Max/min-min distance once. Here we use the spectral method. In particular, the characteristic mean frequency f_n of all the IMFs is estimated by means of the associated Fourier power spectral density $S_n(f)$ as

$$f_n = \frac{\int_0^\infty f S_n(f)\mathrm{d}f}{\int_0^\infty S_n(f)\mathrm{d}f} \tag{3}$$

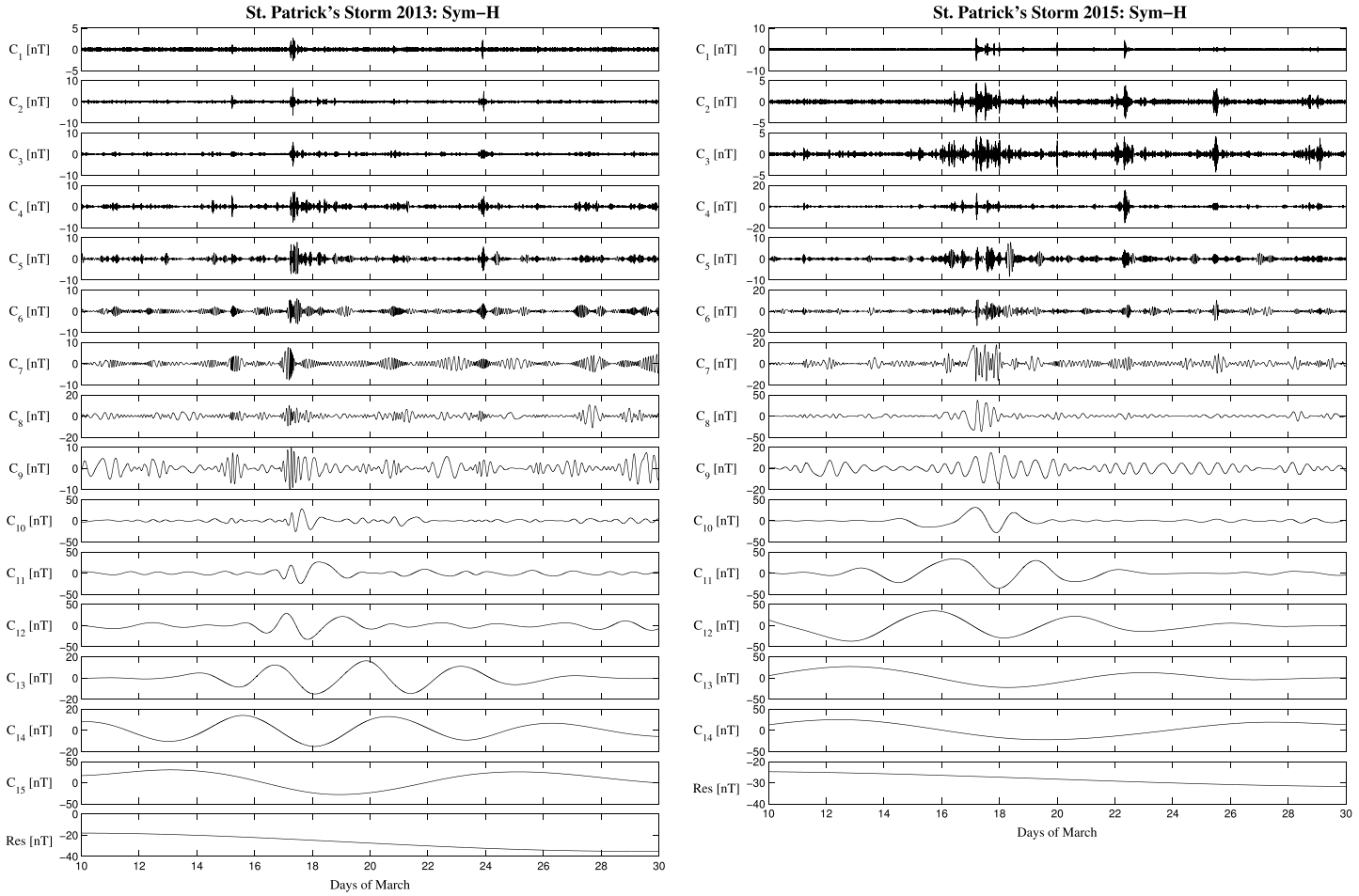

Figure 2. EMD results obtained by analyzing *SYM-H* index for both Storm time periods.

This allows us to obtain the characteristic timescale oscillation of each mode as $\tau_n = f_n^{-1}$. Moreover, since the decomposition is local, complete, and orthogonal, the EMD can be used as a filter by reconstructing partial sums of equation (2) in a chosen frequency range [*Laurenza et al.*, 2012; *Vecchio et al.*, 2012b; *Alberti et al.*, 2014; *De Michelis and Consolini*, 2015].

Figure 4 shows the characteristic frequencies f_n as a function of the mode number n corresponding to the IMFs shown in Figures 2 and 3 relative to *SYM-H* (red circles) and *AE* (blue circles) indices, and to the IMFs obtained from the B_z component (black stars) measured by ACE, for both periods.

2.3. The Delayed Mutual Information (DMI) Approach

In the framework of information theory some different quantities can be estimated to characterize the behavior of a system X or the interference between two systems X and Y. For instance, the *Shannon information entropy* $H(X)$ or the *mutual information* $\mathrm{MI}(X,Y)$ [*Shannon*, 1948] are useful quantities to characterize the behavior of a system X and the degree of statistical independence between two systems (X and Y) by looking to the set of states the systems visit as they evolve in time. In detail, if we indicate as $p(x)$ and $p(x,y)$ the probability of finding a system in state x and the joint probability for the systems X and Y, respectively, then the Shannon information entropy $H(X)$ and the mutual information $\mathrm{MI}(X,Y)$ as follows:

$$H(X) = \sum_{x\in X} p(x) \log \frac{1}{p(x)}, \tag{4}$$

$$\mathrm{MI}(X,Y) = \sum_{x\in X}\sum_{y\in Y} p(x,y) \log \frac{p(x,y)}{p(x)p(y)} \tag{5}$$

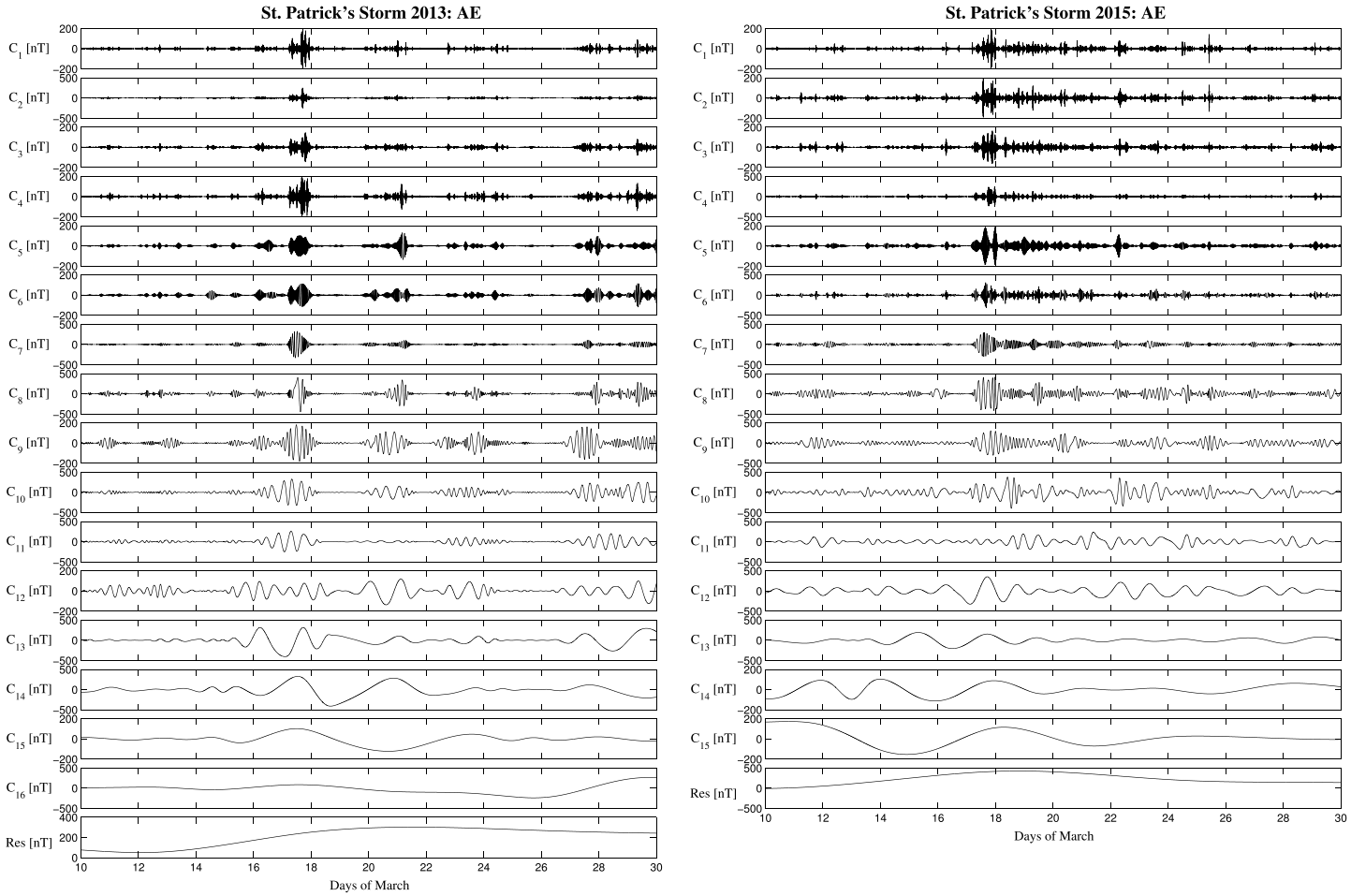

Figure 3. EMD results obtained by analyzing *AE* index for both Storm time periods.

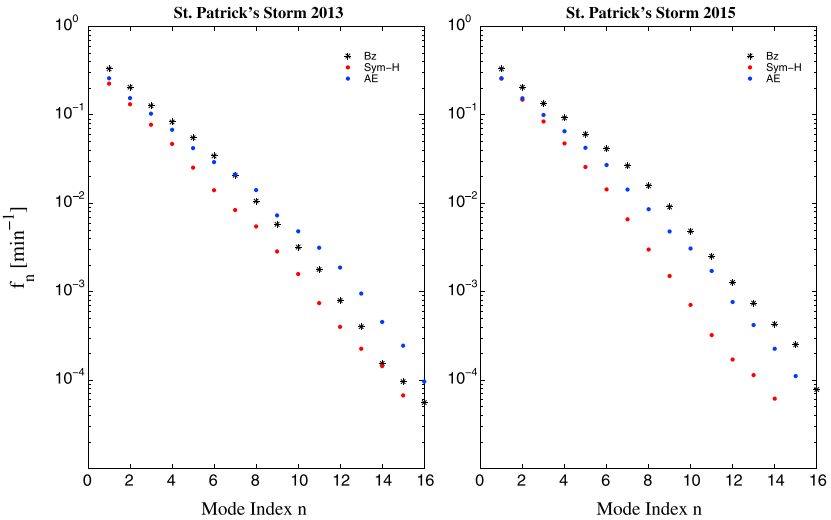

Figure 4. The characteristic frequencies, f_n, versus the mode index, n, for the IMFs relative to B_z (black star), *SYM-H* (red circles), and *AE* (blue circles). IMFs for *SYM-H* and *AE* are reported in Figures 2 and 3, respectively.

Now although the mutual information MI(X, Y) is able to quantify the statistical independence between two signals/systems, no information is provided in an eventual delay of the interference between the two systems X and Y. A better quantity to address this point is the delayed mutual information MI($X, Y \mid \Delta$) (DMI), which is capable of quantifying a time-dependent statistical independence between the two systems. This quantity is defined as follows:

$$\mathrm{MI}(X, Y \mid \Delta) = \sum_{i,j=1}^{N} p_{ij}(X(t), Y(t+\Delta)) \log \frac{p_{ij}(X(t), Y(t+\Delta))}{p_i(X) p_j(Y)} \tag{6}$$

where $p_{ij}(X(t), Y(t+\Delta))$ is the joint probability of observing the couple of values (X, Y), while $p_i(X)$ and $p_j(Y)$ are the probabilities of observing X and Y as independent variables. It can be considered the analog of a cross-correlation function, although it provides an estimation of the total (linear and nonlinear) dependence between two systems/signals [*De Michelis et al.*, 2011] by quantifying the amount of information shared. We underline that the use of DMI to quantify the amount of shared information in the case of SW/IMF parameters and geomagnetic indices is particularly appropriated because of the nonlinear features of the magnetospheric dynamics in response to SW/IMF changes.

To explore the coupling between solar wind (input) and magnetosphere (output) and try to quantify the degree to which one dynamical system affects the dynamics of the other, we use the delayed mutual information MI($X, Y \mid \Delta$).

To quantify the relevance of the dependence/independence degree between two signals using the delayed mutual information MI($X, Y \mid \Delta$), we need to set a significance threshold. This can be done by means of the following procedure. Given two actual time series $\{X_i\}$ and $\{Y_i\}$, an ensemble of $Nr = 10,000$ couples of time series is generated by randomly sorting the two original ones. This operation disrupts any time correlation in each sequence and any possible correspondence between the two time series, without altering the statistics of the values of the actual time series. Hence, for each couple of the randomized time series, we compute the corresponding value of the mutual information MI(X, Y). Then, the statistics of MI(X, Y) values is evaluated by computing the cumulative distribution C(MI). The threshold is chosen at the value $\mathrm{MI}_{\mathrm{thr}}$ for which $C(\mathrm{MI}_{\mathrm{thr}}) = 0.95$. This value corresponds to the 5% confidence limit. If the observed value of MI($X, Y \mid \Delta$) is larger than the threshold $\mathrm{MI}_{\mathrm{thr}}$, we can say that the observed dependence is significative with an error of 5% at the most.

3. Results and Discussion

We start our analysis of the timescale coupling between solar wind parameters and geomagnetic indices by investigating the scale-to-scale DMI between the IMFs of solar wind parameters and that of geomagnetic indices with similar characteristic frequency.

Figure 5 shows the scale-to-scale DMI in the case of the IMFs relative to the interplanetary magnetic field B_z component and the *AE* index for the 2013 St. Patrick's Day storm. This analysis clearly evidences how for timescales $\tau < 200$ min the coupling is not significative, while at timescales $\tau \gtrsim 200$ min the coupling becomes significative for time delays Δ in the range $\Delta \in [0, \sim 600-800)$ min. Furthermore, at these large timescales we observe a maximum of the DMI for a delay $\Delta \sim 100$ min, which is consistent with the propagation time of the perturbation from the ACE L1 position to the internal magnetosphere. To avoid any confusion in what follows, we stress that this delay time is not strictly representative of the response time of the Earth's magnetosphere to SW/IMF changes because it also includes the propagation time.

Similar results are found for the scale-to-scale DMI of other quantities (ϵ, *SYM-H*, AsyH, *AU*, and *AL*) in both the two geomagnetic storms (2013 and 2015 St. Patrick's storms), suggesting that there is a timescale separation in the solar wind-magnetosphere coupling. We observe how this timescale separation occurs at a timescale $\tau \simeq 200$ min, which is in a good agreement with the typical timescale discerning direct driven and loading-unloading magnetospheric processes [*Kamide and Kokubun*, 1996; *Consolini and De Michelis*, 2005]. When referring to fluctations at a certain timescale, the term "direct driven" here is intended according to the linear response theory, i.e., a correspondence between input and output fluctuations at the different timescales unless of a linear filtering.

Moving from this observation of a clear timescale separation for the coupling, we reconstruct two different signals using the EMD. In detail, we divide each set of modes into two subsets: (i) a short-timescale set, with characteristic timescales $\tau \lesssim 200$ min, and (ii) a long-timescale one, with $\tau \gtrsim 200$ min.

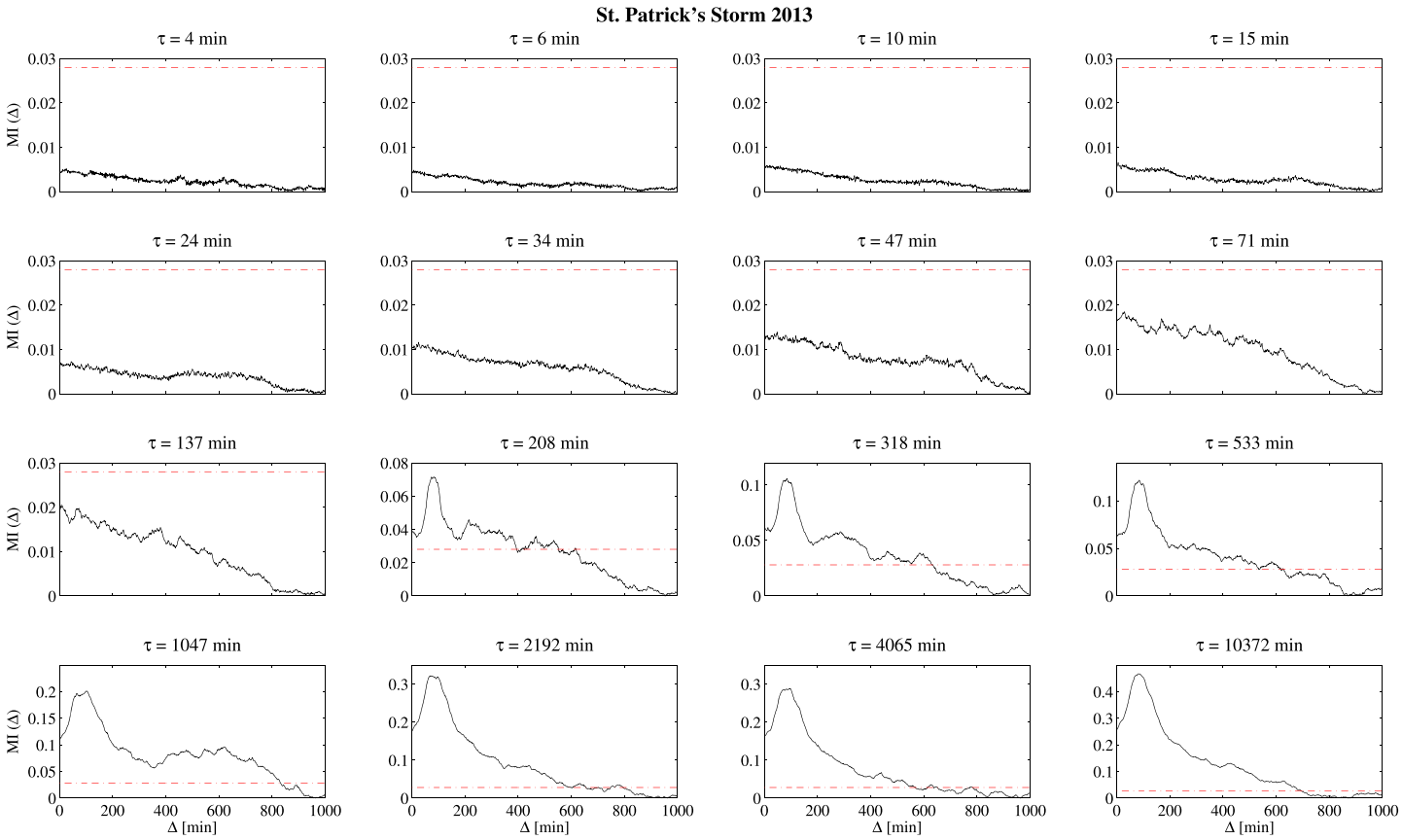

Figure 5. The scale-to-scale DMI between IMFs of the interplanetary magnetic field B_z component and auroral electroject *AE* index for the St. Patrick's storm 2013 time period. Red dashed line indicates the significance (5% null hypothesis) DMI threshold, $MI_{thr} = 0.028$.

Figures 6 and 7 show an example of the reconstructed short- and long-timescale signals in comparison with the actual one for the *AE* index relative to the 2013 St. Patrick's Day storm and the corresponding Fourier spectrum (PSD), respectively. In particular, the PSD clearly shows the relative contribution of the two reconstructed signals to the total PSD of the actual time series, with a frequency cutoff occurring at $f_c \sim 5 \times 10^{-3}$ min^{-1}. Although the EMD can be thought to act as a low-/high-pass filter, when separating the short- and long-timescale fluctuations, it does not alter the phases of the different spectral contributions, in contrast to standard Fourier-based filters.

The DMI analysis is, then, performed on the reconstructed short- and long-timescale signals relative to the interplanetary magnetic field B_z component and the *AE* index for the 2013 St. Patrick's Day storm. As shown in Figure 8, a clear and significant amount of shared information (correlation) is found in the case of the long-timescale signals with a maximum of the DMI for a time delay $\Delta \sim 100$ min. Conversely, in the case of short-timescale signals the observed correlation is not significant, indicating that it is reasonable to assume that the processes responsible for the dynamics of Earth's magnetosphere at these timescales are not directly driven by the solar wind parameters. The observed absence of a significative correlation at timescales shorter than 200 min could be due to a *random phase* effect as a consequence of the fact that ACE data have not been adjusted to account for the propagation time between L1 point and the bow shock nose. This random phase effect (acting as a *jitter*) could, indeed, smear out some significant correlation. To check if this hypothesis/interpretation is reasonable, we have attempted two different approaches to correct the results at timescales below 200 min: (i) a OMNI-based propagation method and (ii) a fluid-like based propagation method. Both the two methods (which are discussed in detail in Appendix A) do not produce any significative change in the meaningfulness of the above results (please refer to Appendix A). The main effect of the propagation is the reduction of the time delay Δ in correspondence of which the DMI is maximal. In particular, we get a maximum of the DMI for a time delay of $\Delta \sim 50-70$ min. Furthermore, conversely to what is expected, the meaningfulness of DMI at timescales shorter than 200 min does not show any significative change, as it is

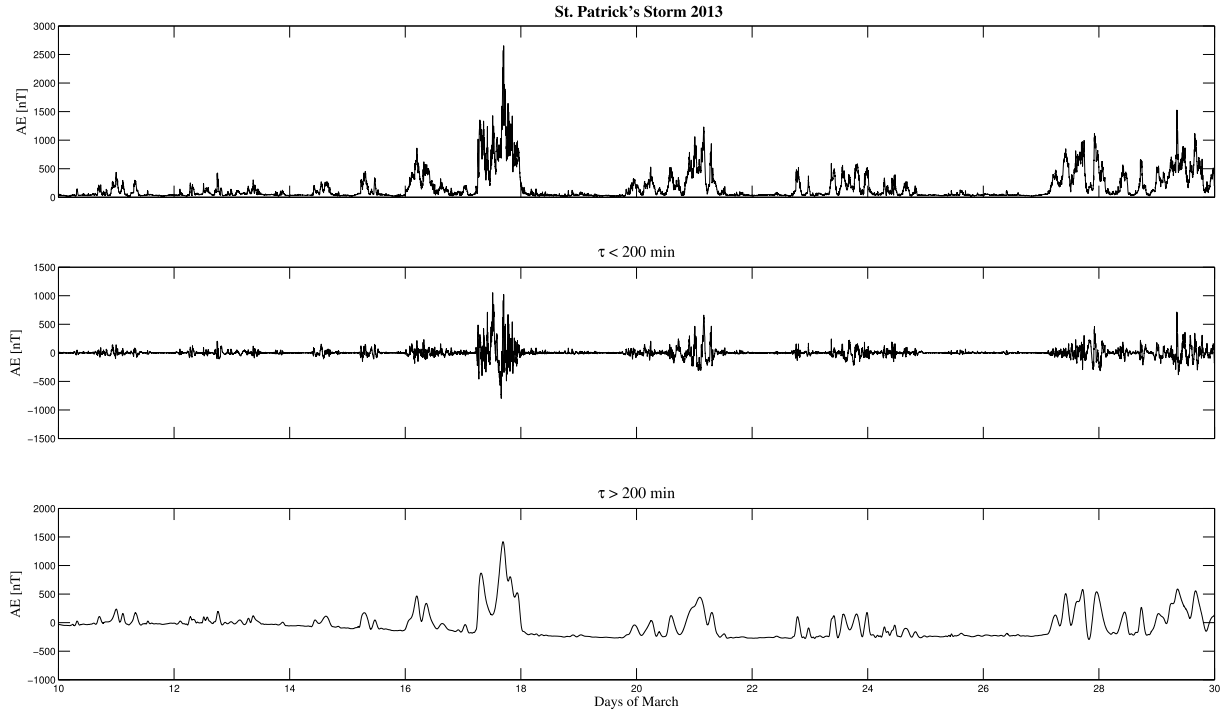

Figure 6. (top) The actual, (middle) the short-timescale ($\tau < 200$ min), and (bottom) the long-timescale ($\tau > 200$ min) signals of *AE* index for the St. Patrick's storm 2013 time period.

for the timescales longer than 200 min. These results suggest that the Earth's magnetospheric dynamics play a very relevant role at timescales shorter than 200 min, confirming what has been extensively documented in several previous works [*Tsurutani et al.*, 1990; *Kamide and Kokubun*, 1996; *Consolini*, 1997; *Sitnov et al.*, 2001; *Uritsky et al.*, 2002; *Consolini and De Michelis*, 2005].

To better investigate this point we extend the above analysis to all the other parameters considered in this work and also for the St. Patrick's Day storm that occurred in 2015.

Figure 9 shows the results of the DMI analysis for the actual and reconstructed time series in the case of *SYM-H*, *ASY-H*, *AU*, and *AL* versus IMF B_z component, and *SYM-H*, *ASY-H*, *AE*, *AU*, and *AL* versus the Perrault-Akasofu coupling function ϵ. All the cases confirm the previous results. Timescales longer than 200 min are directly

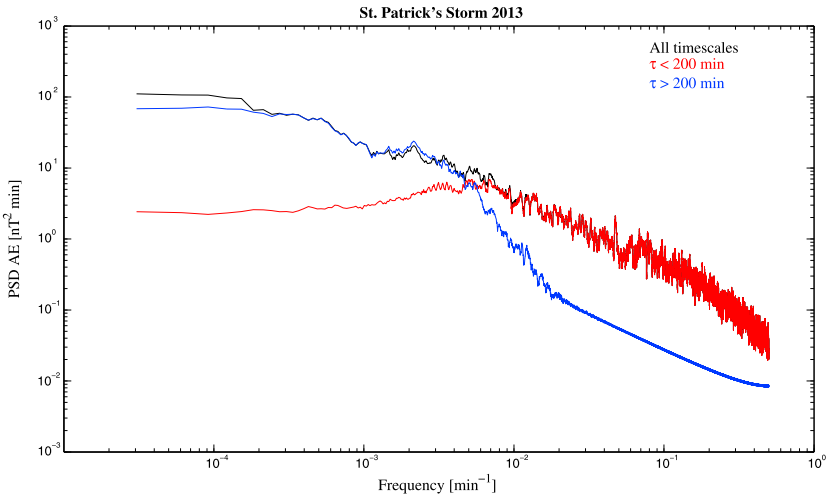

Figure 7. The PSD of the actual and reconstructed signals of *AE* index for the St. Patrick's storm 2013 time period. Black, red, and blue lines refer to actual, short-timescale ($\tau < 200$ min), and long-timescale ($\tau > 200$ min) signals, respectively.

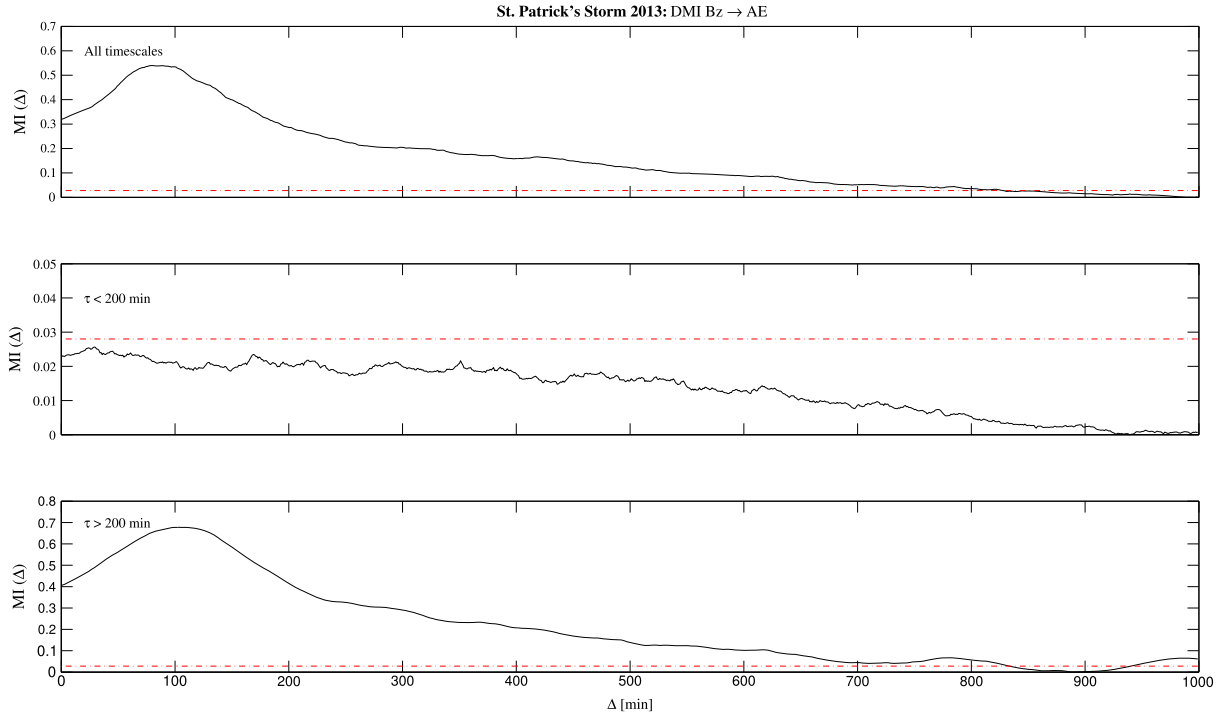

Figure 8. The DMI analysis between IMFs of the interplanetary magnetic field B_z component and auroral electroject *AE* index for (top) the actual, (middle) the short-timescale ($\tau < 200$ min), and (bottom) the long-timescale ($\tau > 200$ min) signals for the 2013 St. Patrick's storm time period. The dashed red line is the significance (5% null hypothesis) DMI threshold, $MI_{thr} = 0.028$.

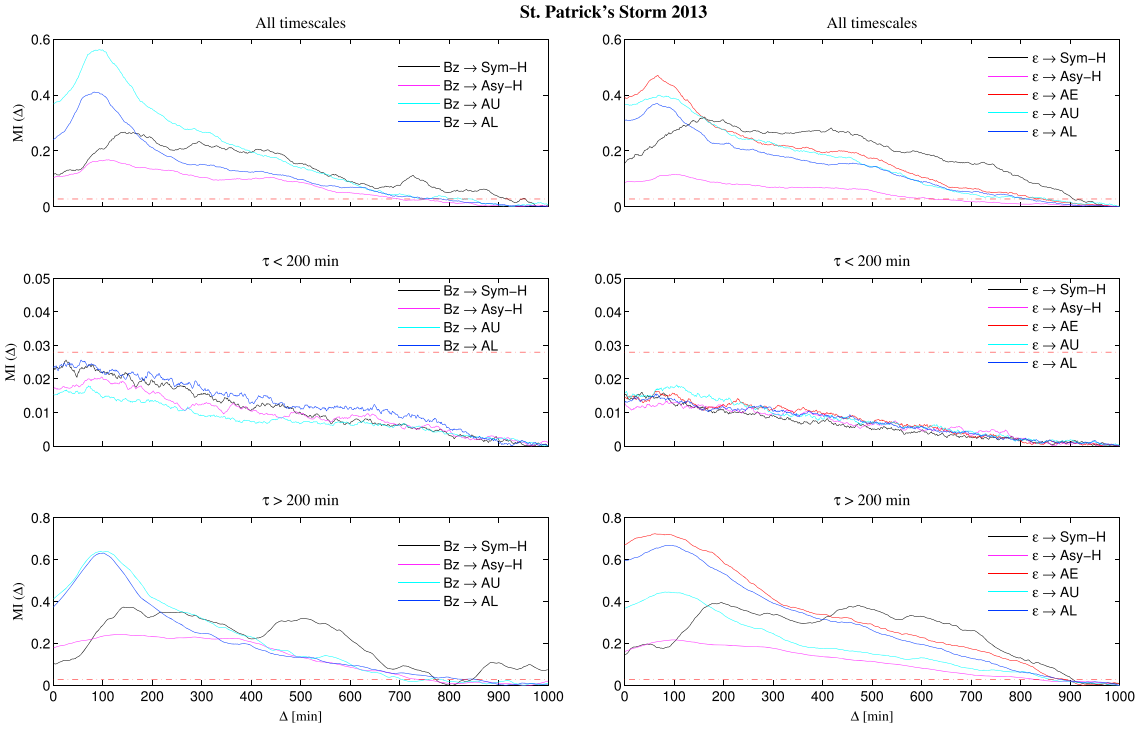

Figure 9. The DMI results on different timescales between solar wind IMF B_z component, the Perrault-Akasofu coupling function, ϵ, and magnetospheric response proxies, *SYM-H*, *ASY-H*, *AE*, *AU*, and *AL*, for the 2013 St. Patrick's storm time period. The dashed red line represents the significance (5% null hypothesis) DMI threshold, $MI_{thr} = 0.028$.

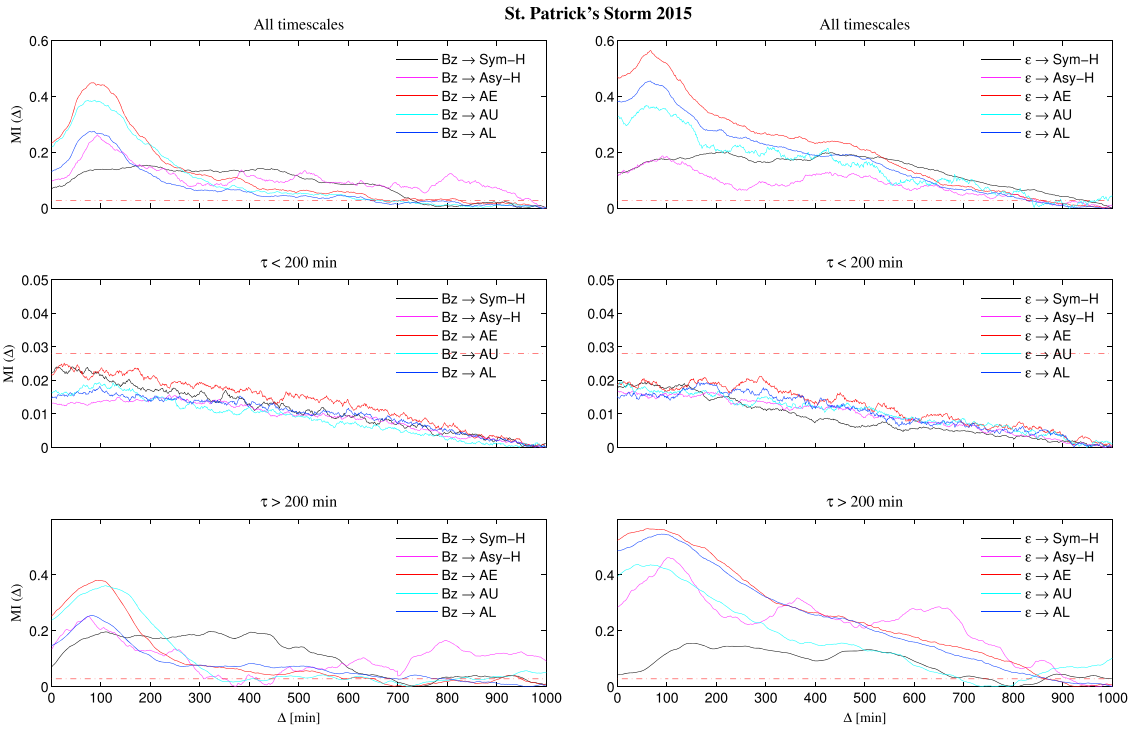

Figure 10. As in Figure 9 for the 2015 St. Patrick's storm time period.

coupled to (driven by) solar wind, while for timescales shorter than 200 min, there is no direct coupling to solar wind parameter fluctuations. The same results are found in the case of the 2015 St. Patrick's Day storm as shown in Figure 10.

Another interesting feature emerging from our analysis is how at long timescales the response of the magnetospheric ring current, as monitored by *SYM-H*, is delayed with respect to the high-latitude electrojet current systems. Indeed, while for high-latitude geomagnetic indices (*AE*, *AU*, and *AL*) the maximum of the MI(Δ) is found in correspondence of Δ ∼ 100 min (Δ ∼ 70–80 min for ACE-propagated data), *SYM-H* responds later being Δ ∼ 150–200 min (Δ ∼ 100–150 min for ACE-propagated data). A more different behavior is shown by *ASY-H*, which indeed shows a maximum of the MI(Δ) for a time delay of Δ ∼ 100 min (Δ ∼ 60–80 min for ACE-propagated data), i.e., a time delay similar to the high-latitude geomagnetic indices. This result confirms the previous findings by *Crooker* [1972] and *Clauer and McPherron* [1980] that showed that the asymmetric part of the variation of the horizontal component *H* of geomagnetic field at low latitude well correlates with the general trend of the auroral electrojet index *AE*. Furthermore, the time delay corresponding to the DMI maximum observed in the case of *AE* indices and *ASY-H* seems to be well in agreement with the time necessary to the interplanetary disturbance (CME) to propagate from L1 (ACE) to the magnetopause plus the typical ∼64–72 min of the median growth-phase period of southward IMF preceding a classical substorm [see, e.g., *Lyons et al.*, 1997]. The explanation of this point has to be found in the link between the development of the partial ring current and the increase of the dawn-dusk interplanetary electric field. Conversely, the possible explanation of this different response time delay observed in the case of *SYM-H* suggests that the ring current enhancement requires a longer time, this being related to the time for plasma to be convected/advected to the Earth's distances in the inner regions of the magnetosphere where the ring current is located.

Finally, the absolute and maximum values of the shared information MI at long timescales are generally higher for geomagnetic high-latitude indices (*AE*, *AU*, and *AL*) than for *SYM-H* and *ASY-H*. This suggests that there could be inner physical processes that tend to reduce the correlation between *SYM-H* and *ASY-H* and external drivers.

4. Summary and Conclusions

In this work, we have presented a detailed analysis of the response of the Earth's magnetosphere to solar wind disturbances in terms of timescale coupling during two major geomagnetic storms, the 2013 and 2015 St. Patrick's Day storms. Our analysis is based on novel approaches, the EMD and the DMI, which allow to separate fluctuations at different timescales contributing to a signal and to analyze the linear/nonlinear interference/coupling between two signals.

The main results of our work can be summarized as follows:

1. The magnetospheric short-timescale fluctuations seem to be not directly related to the same timescale fluctuations in the SW/IMF, because the MI is under the null hypothesis threshold. This is a relevant result indicating that internal magnetospheric processes strongly affect the magnetospheric response at timescales lower than 200 min in the magnetospheric dynamics. With the term "internal origin" we mean that there is not a one-to-one coupling. Anyway, the transient activities at these timescales (see, e.g., the bursty enhancement of high-latitude electrojet currents, the occurrence of fast relaxation processes in the tail regions, such as bursty bulk flows) that are responsible for the fast variations observed in the geomagnetic indices at short timescales, are certainly triggered by IMF and solar wind changes but do not seem directly driven in terms of fluctuations.
2. On the contrary, the SW/IMF fluctuations at long timescales play a primary role into the coupling of timescales greater than 200 min in the magnetosphere. This indicates that the magnetospheric response to the SW/IMF driver at these timescales is well correlated, suggesting that direct driven processes are responsible for the geomagnetic indices fluctuations at these timescales.
3. A time delay of $\Delta \sim 100-150$ min ($\Delta \sim 70-80$ min for ACE-propagated data) is found between solar wind/IMF parameters (observed at L1 position) and magnetospheric overall dynamics (measured by indices), which is quite well in agreement with the travel time necessary to the SW/IMF perturbation to propagate from the ACE spacecraft position to the Earth's magnetopause plus the response time of the Earth's magnetosphere for the occurrence of storms/substorms.
4. A great information transfer can be observed between IMF B_z component and *AE*, *AU*, and *AL* indices, while a lower transfer is found when IMF B_z component and *SYM-H*/*ASY-H* are considered.

Although in this work we have limited our discussion to the role that IMF B_z and the Perrault-Akasofu coupling function ϵ play, we remark that the same analyses have been performed to other solar wind parameters: the solar wind dynamic pressure p_{SW}, the velocity flow v, vB_{South}, and the Newell coupling function $d\Phi_{MP}/dt$ [*Newell et al.*, 2007] (not shown here). The obtained results do not show any substantial difference from those reported in this work.

Our findings support the common idea that the Earth's magnetosphere response consists of both direct driven and internal processes, where the internal processes can be considered more reasonably as only triggered by external solar wind changes. Furthermore, there is a clear separation of timescales between the internal processes and the direct driven ones, being the characteristic separation timescale of the order of 100–200 min. This timescale separation is well in agreement with previous findings on loading-unloading typical timescales [*Kamide and Kokubun*, 1996; *Consolini and De Michelis*, 2005] and also with typical timescales involved in the nonlinear response of the Earth's magnetosphere [*Tsurutani et al.*, 1990]. Furthermore, the smaller MI maximum value for *SYM-H* could be due to the effect that internal processes (like loading-unloading ones taking place in the central plasma sheet of the magnetotail region) play on the enhancement of the Earth's ring current. We remind that part of the Earth's ring current enhancement during geomagnetic storms is due to high-latitude ionospheric ion species (typically oxygen O^+) outflowing as a consequence of FAC activation [*Daglis et al.*, 1994].

The observed absence of coupling (direct inference) between Earth's magnetospheric short timescales and the corresponding solar wind ones supports the inherent difficulties in forecasting high-latitude geomagnetic disturbances, as monitored by auroral electrojet index *AE*, using artificial neural networks based on IMF and solar wind parameters at timescales shorter than 1 h [*Pallocchia et al.*, 2007]. The fluctuations at these timescales, although triggered by the transfer of external energy, mass, and momentum, are not mainly directly coupled to the solar wind parameter fluctuations but result from a complex interplay of external and internal processes. Consequently, a better forecasting of processes occurring on fast timescales requires to

find a valid proxy of the internal magnetosphere dynamical state, with a special attention to the state of the Earth's magnetotail plasma sheet. These can be useful for Space Weather prediction models.

In conclusion, our analysis of relevant coupling timescales during geomagnetic storms and substorms by using both EMD and DMI methods evidenced additional aspects of the solar wind-magnetosphere coupling because (i) a nonstationary and nonlinear analysis can be carried out by using the EMD without any a priori assumptions on the decomposition basis (as for less novel techniques), (ii) the scale-to-scale DMI analysis shows a quantitative evidence of the existence of a timescale separation in solar wind-magnetosphere coupling, and (iii) differently from linear cross-correlation analysis, the DMI performs total linear and nonlinear correlation analysis.

Appendix A: Effect of Propagation From L1 to Bow Shock Nose

A1. OMNI-Based Propagation Method

One way to study solar wind properties at the bow shock nose position is to use the OMNI database. The shift procedure is based on single spacecraft measurements made by ACE and WIND, shifted by assuming that solar wind variations are organized in series of phase fronts, convecting with the solar wind bulk speed. In this way, the time shift equation is

$$\delta t = \frac{\vec{n} \cdot \left(\vec{R}_d - \vec{R}_o\right)}{\vec{n} \cdot \vec{V}} \tag{A1}$$

where $\vec{n}$ is the variation phase front normal (PFN), $\vec{R}_d$ is the bow shock position, $\vec{R}_o$ is the spacecraft position (L1), and $\vec{V}$ is the solar wind velocity. To determine normals to discontinuity planes in the solar wind magnetic field, a modified version of the minimum variance analysis (MVA) technique is used (see *Weimer et al.* [2003], *Bargatze et al.* [2005], *Haaland et al.* [2006], and *Weimer and King* [2008], for more details). The MVA is only applied on magnetic field data, although the location of the bow shock nose $\vec{R}_d$ requires the knowledge of other solar wind parameters such as velocity, proton and alpha particle densities, proton temperature, and ram pressure. Indeed, it is assumed that the geocentric direction to the bow shock nose is parallel to the solar wind flow direction (a correction is needed to take into account mean orbital speed of the Earth around the Sun) such that

$$|\vec{R}_d| = R_{\mathrm{mp}} \left[1.0 + 1.1 \frac{\frac{2}{3}M^2 + 2}{\frac{8}{3}(M^2 - 1)}\right] \tag{A2}$$

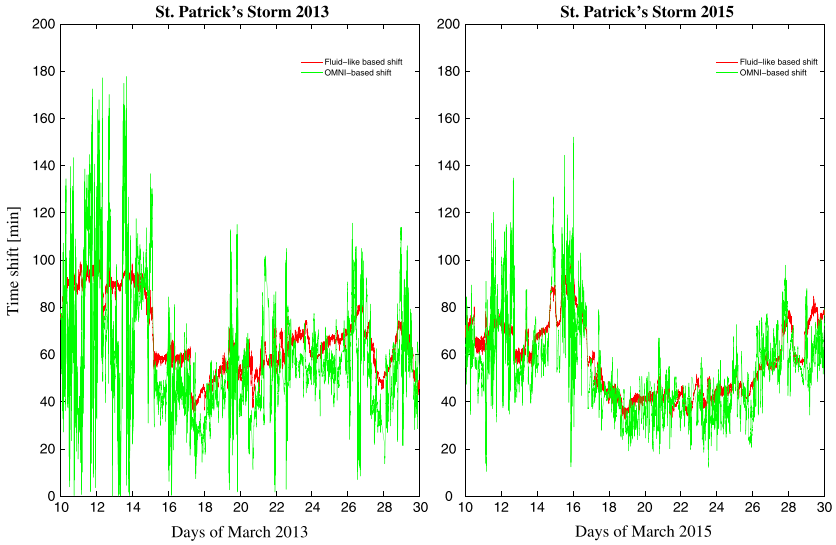

Figure A1. Time shifts obtained with the two different methods described in Appendix A for both St. Patrick's Day storms in 2013 and 2015. Green line refers to the OMNI-based shift procedure as in section A1, while red line shows the time shift obtained via the procedure as in section A2.

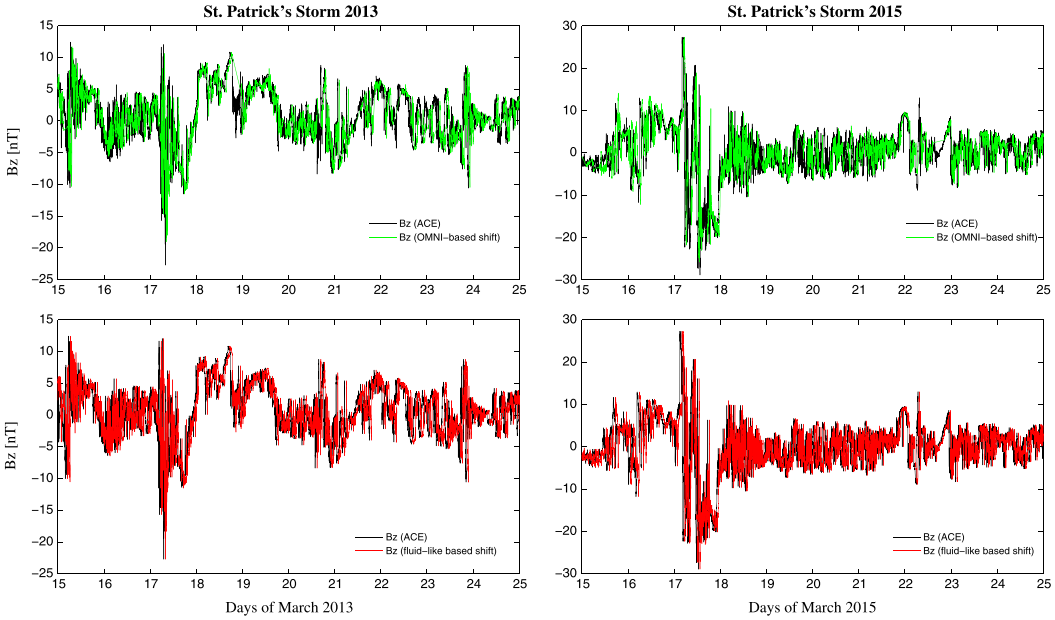

Figure A2. Time behavior of the interplanetary magnetic field B_z component as obtained from raw data by ACE and by using both time shift propagation methods. Black lines refer to the observed values (i.e., ACE data), green lines to OMNI-based time-shifted data and red line to fluid-like based time-shifted data. We zoom over the time interval 15–25 March in both cases for a more convenient visual inspection.

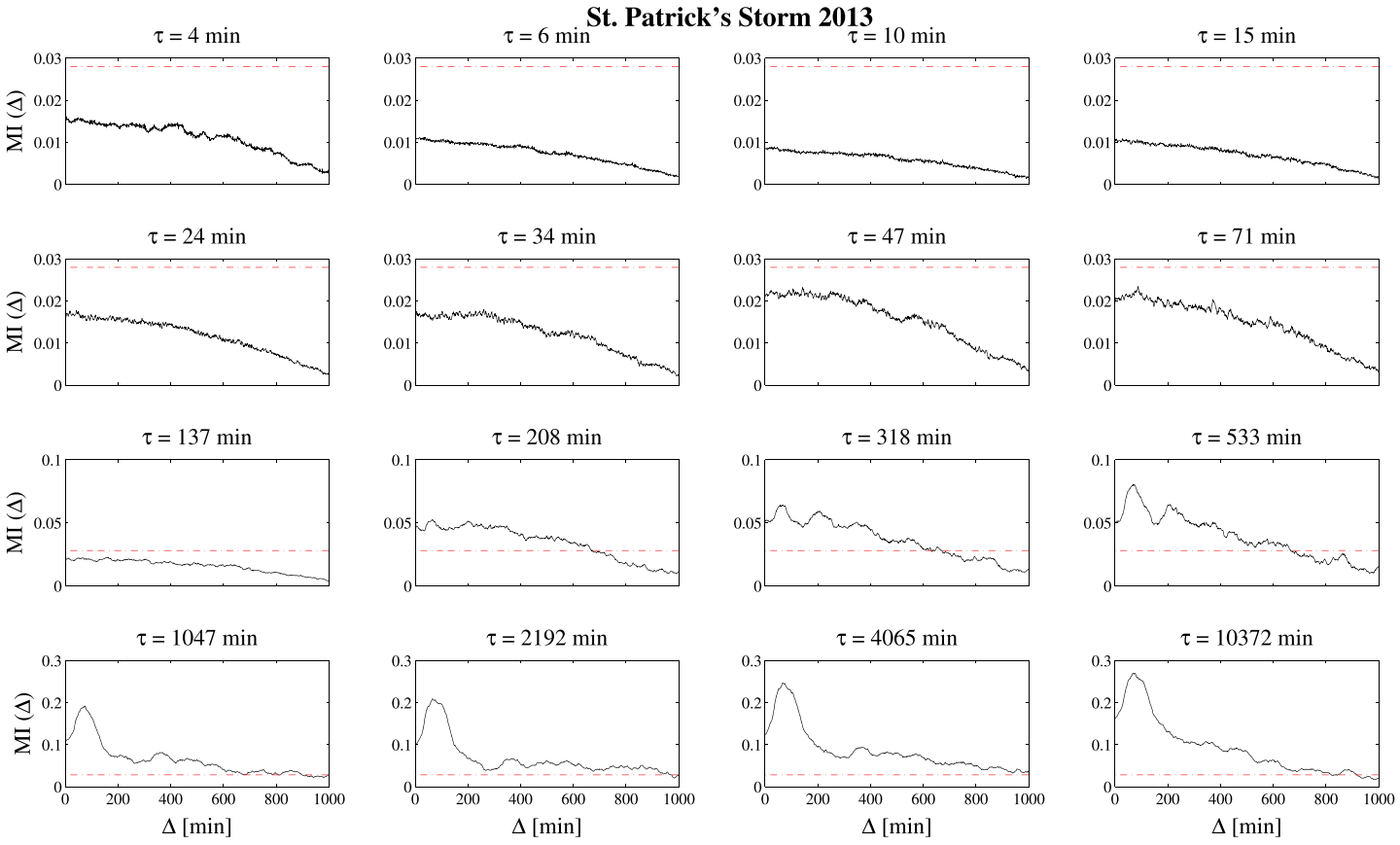

Figure A3. The scale-to-scale DMI between IMFs of the fluid-like based shifted ACE B_z component and auroral electroject *AE* index for the St. Patrick's storm 2013 time period. Red dashed line indicates the significance (5% null hypothesis) DMI threshold, $MI_{thr} = 0.028$.

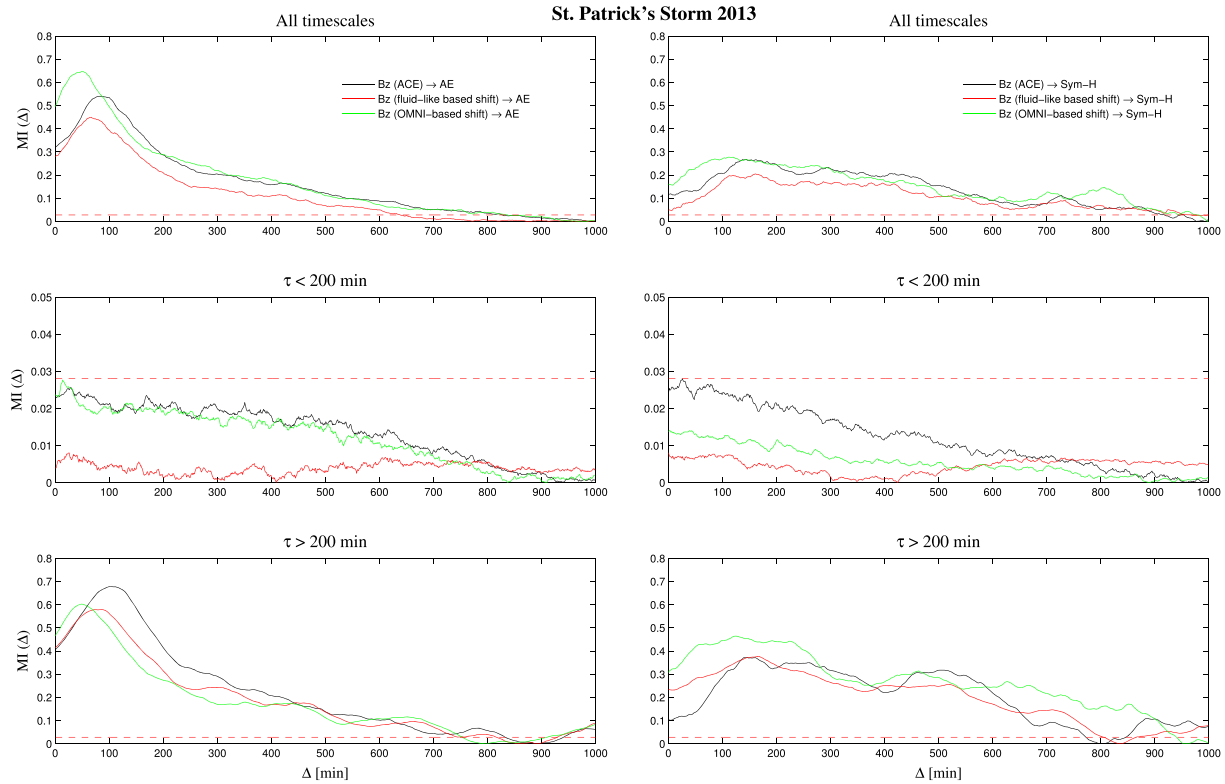

Figure A4. The DMI analysis between IMFs of the interplanetary magnetic field B_z component and auroral electroject *AE* index for (top row) the actual, (middle row) the short-timescale ($\tau < 200$ min), and (bottom row) the long-timescale ($\tau > 200$ min) signals for the 2013 St. Patrick's storm time period. Black line is related to the DMI applied by using observed value of B_z by ACE, while green and red lines refer to the different time shift methods used. The dashed red line is the significance (5% null hypothesis) DMI threshold, $\mathrm{MI}_{\mathrm{thr}} = 0.028$.

with

$$M = \frac{V_{\mathrm{sw}}}{V_{\mathrm{ms}}} \tag{A3}$$

$$V_{\mathrm{ms}} = \sqrt{0.5\left\{V_A^2 + V_s^2 + \sqrt{\left[\left(V_A^2 + V_S^2\right)^2 + 4(V_A^2 V_S^2 \cos^2(\theta)\right]}\right\}} \tag{A4}$$

$$V_A = \frac{B}{\sqrt{4\pi(4N_a + N_p)M_p}} \tag{A5}$$

$$V_s = 0.12\sqrt{T_p + 1.28 \times 10^5} \tag{A6}$$

$$R_{\mathrm{mp}} = (11.4 + KB_z)P^{-1/6.6} \tag{A7}$$

$$P = (2 \times 10^{-6})N_p V_p^2 \tag{A8}$$

where R_{mp} is the geocentric magnetopause nose distance, M is the magnetosonic Mach number, V_{ms} is the magnetosonic speed, V_A is the Alfven speed, V_S is the sound speed, θ is the angle between $\vec{B}$ and $\vec{v}$, N_a and N_p are the alpha particle and proton densities, M_p is the proton mass, T_p is the proton temperature, V_p is the proton velocity, and P is the pressure.

Nevertheless, the time shift procedure is built up by making a "rigid" time shift between the L1 and the nose of the bow shock positions that does not consider the "real" solar wind structure propagation. Indeed, solar wind streams can interact and generate new types of structures which cannot be simply monitored by "rigidly" shifting solar wind parameter values. As also pointed out by OMNI documentation

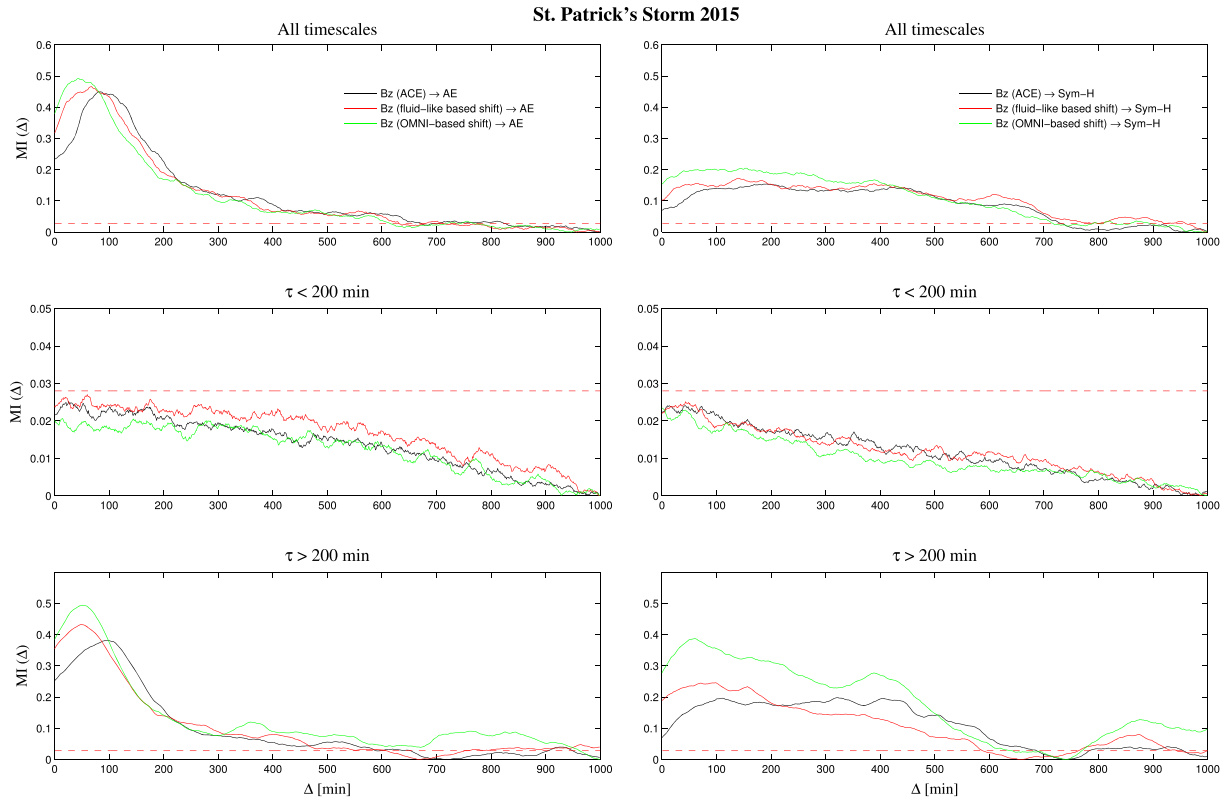

Figure A5. As in Figure A4 for the 2015 St. Patrick's storm time period.

(http://omniweb.gsfc.nasa.gov/html/HROdocum.html) their time shift technique "is a very simplified approach, neglecting finite response times of the magnetosphere to solar wind variations, that may introduce some errors." Additional details about OMNI procedure can be found at http://omniweb.gsfc.nasa.gov/html/HROdocum.html.

A2. Fluid-Like Based Propagation Method

We try to propagate, in a "fluid" sense, different from the "wave-like" propagation made by OMNI (by using shock front direction), ACE spacecraft data. We built up a procedure characterized by the following steps: (i) we identified the direction of the relative positions of ACE spacecraft and bow shock nose ($\vec{r}$), (ii) we projected the solar wind velocity vector measured by ACE ($\vec{v}$) on that direction, and (iii) we evaluate the corresponding time shift as

$$\tau_s = \frac{|\vec{r}|}{\vec{v} \cdot \vec{r}} \tag{A9}$$

where $\vec{r} = \vec{R}_d - \vec{R}_o$ in which the bow shock nose position $\vec{R}_d$ is calculated as in equation (A2). Similarly to the OMNI shifting procedure, we used "Level 2" 16 s magnetic field data and 64 s plasma data obtained by ACE to evaluate both the location of the bow shock nose $\vec{R}_d$ and the "fluid-like" time shift (equation (A9)). Then, we applied the same procedure developed by OMNI to shift time series, i.e., by changing their time tags and resampling time series at 1 min. As for the OMNI procedure, our approach is based on "rigid" time shift, without any consideration of the "in situ" solar wind structure generation. Indeed, the solar wind is a complex system in which several processes can develop and the bow shock surface is not "static" but it is continuously modified by the solar wind itself. This problem could be solved by making the necessary time shift, which implies a complete knowledge of the solar wind properties at L1 position and, simultaneously, the bow shock properties, including magnetic field topology and geometry (this cannot be correctly done since only two satellites are present at L1 and a "topological and geometrical view" of solar wind structures is not possible). Moreover, we should also know the properties of the heliospheric medium between L1 and the bow shock nose positions, since, as stated above, several structures can be generated "in situ" due to solar wind streams interaction and a correct estimation of their formation is not possible by only using spacecraft data

from L1 position. A solution of this problem could be found if we had a numerical model for the bow shock position and also for each solar wind structure in order to investigate its evolution in the heliospheric medium between L1 and bow shock nose positions.

A3. Effect on DMI Analysis

Using the two methods described in the previous sections, we have computed the time shifts for the two geomagnetic storms under consideration. The obtained time shifts for both St. Patrick's Day storms in 2013 and 2015, which are shown in Figure A1, allow us to reconstruct propagated (time shifted) signals (see Figure A2) to which we can apply all the same analysis described in the text to compute the DMI.

Similarly to Figure 5, Figure A3 shows the scale-to-scale DMI in the case of the IMFs relative to the fluid-like shifted B_z component and the *AE* index for the 2013 St. Patrick's Day storm. This analysis confirms that for timescales $\tau < 200$ min the coupling is not significant, while at timescales $\tau \gtrsim 200$ min the coupling becomes significant for time delays Δ in the range $\Delta \in [0, \sim 600-800)$ min, with a maximum of the DMI for a delay $\Delta \sim 60-70$ min.

Moving from these observations, in Figures A4 and A5 we report the results of the DMI analysis between B_z and *AE* or *SYM-H* for the 2013 and 2015 St. Patricks's storms, respectively. The results clearly show the following:

1. A reduction of the time delay Δ from $\sim 100-150$ min to $\sim 70-80$ min. The observed time delay for propagated data is well in agreement with what was generally reported in the literature [see, e.g., *Lyons et al.*, 1997].
2. The absence of a significative correlation at timescales shorter than 200 min, which confirms the previous results on the meaningfulness of DMI at these timescales.
3. An increase of the value of the DMI maximum value for OMNI-based shifted data when all the timescales are considered. This is generally true also at timescales larger than 200 min.

The same results have been found also for the other interplanetary quantities considered in this work.

Acknowledgments

This research work is partly supported by the Italian MIUR-PRIN grant 2012P2HRCR on *The active Sun and its effects on Space and Earth climate*, and by Space Weather Italian Community (SWICO) Research Program. The authors acknowledge J.H. King and N. Papatashvilli at NASA and CDA Web for solar wind data. Acknowledgments are also due to N. Ness of Bartol Research Institute, PI of ACE magnetic field instrument, and to D.J. McComas of Southwest Research Institute, PI of ACE/SWEPAM Solar Wind Experiment. The OMNI data were obtained from the GSFC/SPDF OMNIWeb interface at http://omniweb.gsfc.nasa.gov. The authors also acknowledge World Data Center for Geomagnetism (Kyoto) for the use of the geomagnetic indices data. The EMD code used for the analysis was developed by A. Vecchio. All the derived data products presented in this paper are available upon request by email to the authors (tommaso.alberti@unical.it).

References

Ahn, B. H., S. I. Akasofu, and Y. Kamide (1983), The Joule heat production rate and the particle energy injection rate as a function of the geomagnetic indices *AE* and *AL*, *J. Geophys. Res.*, *88*, 6275–6287.

Akasofu, S. I. (1983), Solar-wind disturbances and the solar wind-magnetosphere energy coupling function, *Space Sci. Rev.*, *34*, 173–183.

Alberti, T., F. Lepreti, A. Vecchio, E. Bevacqua, V. Capparelli, and V. Carbone (2014), Natural periodicities and Northern Hemisphere-Southern Hemisphere connection of fast temperature changes during the last glacial period: EPICA and NGRIP revisited, *Clim. Past*, *10*, 1751–1762, doi:10.5194/cp-10-1751-2014.

Alberti, T., M. Piersanti, A. Vecchio, P. De Michelis, F. Lepreti, V. Carbone, and L. Primavera (2016), Identification of the different magnetic field contributions during a geomagnetic storm in magnetospheric and ground observations, *Ann. Geophys.*, *34*, 1069–1084, doi:10.5194/angeo-34-1069-2016.

Bargatze, L. F., R. L. McPherron, J. Minamora, and D. Weimer (2005), A new interpretation of Weimer et al's solar wind propagation delay technique, *J. Geophys. Res.*, *110*, A07105, doi:10.1029/2004JA010902.

Consolini, G. (1997), Sandpile cellular automata and the magnetospheric dynamics, in *Cosmic Physics in the Year 2000, Proceedings of 8th GIFCO Conference*, vol. 58, edited by S. Aiello et al., pp. 123–126, SIF, Bologna, Italy.

Consolini, G. (2002), Self-organized criticality: A new paradigm for the magnetotail dynamics, *Fractals*, *10*, 275–283.

Consolini, G., and T. S. Chang (2001), Magnetic field topology and criticality in geotail dynamics: Relevance to substorm phenomena, *Space Sci. Rev.*, *95*, 309–321.

Consolini, G., and P. De Michelis (2005), Local intermittency measure analysis of *AE* index: The directly driven and unloading component, *Geophys. Res. Lett.*, *32*, L05101, doi:10.1029/2004GL022063.

Consolini, G., and P. De Michelis (2011), Rank ordering multifractal analysis of the auroral electroject index, *Nonlinear Processes Geophys.*, *18*, 277–285.

Consolini, G., and P. De Michelis (2014), Permutation entropy analysis of complex magnetospheric dynamics, *J. Atmos. Sol. Terr. Phys.*, *115–116*, 25–31, doi:10.1016/j.jastp.2013.11.005.

Consolini, G., M. F. Marcucci, and M. Candidi (1996), Multifractal structure of auroral electroject index data, *Phys. Rev. Lett.*, *76*, 4082–4085.

Consolini, G., P. De Michelis, and R. Tozzi (2008), On the Earth's magnetospheric dynamics: Nonequilibrium evolution and the fluctuation theorem, *J. Geophys. Res.*, *113*, A08222, doi:10.1029/2008JA013074.

Clauer, C. R., and R. L. McPherron (1980), The relative importance of the interplanetary electric field and magnetospheric substorms on partial ring current development, *J. Geophys. Res.*, *85*, 6747–6759.

Clauer, C. R., R. L. McPherron, and C. Searles (1983), Solar wind control of the low latitude asymmetric magnetic disturbance field, *J. Geophys. Res.*, *88*, 2123–2130.

Crooker, N. C. (1972), High-time resolution of the low-latitude asymmetric disturbance in the geomagnetic field, *J. Geophys. Res.*, *77*, 773–775.

Crooker, N. C., and G. L. Siscoe (1971), A study of geomagnetic disturbance field asymmetry, *Radio Sci.*, *6*, 495–501.

Daglis, L. A., S. Livi, E. T. Sarris, and B. Wilken (1994), Energy density of ionospheric and solar wind origin ions in the near-Earth magnetotail during substorms, *J. Geophys. Res.*, *99*, 5691–5703.

Davies, T. N., and M. Sugiura (1966), Auroral electrojet activity index *AE* and its universal time variations, *J. Geophys. Res.*, *71*, 785–801.

De Michelis, P., and G. Consolini (2015), On the local Hurst exponent of geomagnetic field fluctuations: Spatial distribution for different geomagnetic activity levels, *J. Geophys. Res. Space Physics*, *120*, 2691–2701, doi:10.1002/2014JA020685.

De Michelis, P., G. Consolini, M. Materassi, and R. Tozzi (2011), An information theory approach to the storm-substorm relationship, *J. Geophys. Res.*, *116*, A08225, doi:10.1029/2011JA016535.
De Michelis, P., G. Consolini, and R. Tozzi (2012), On the multi-scale nature of large geomagnetic storms: An empirical mode decomposition analysis, *Nonlinear Process Geophys.*, *19*, 667–673.
De Michelis, P., G. Consolini, and R. Tozzi (2015), Latitudinal dependence of short timescale fluctations during intense geomagnetic storms: A permutation entropy approach, *J. Geophys. Res. Space Physics*, *120*, 5633–5644, doi:10.1002/2015JA021279.
Finch, I., and M. Lockwood (2007), Solar wind-magnetosphere coupling functions on timescales of 1 day to 1 year, *Ann. Geophys.*, *25*, 495–506.
Haaland, S., G. Paschmann, and B. U. Ö. Sonnerup (2006), Comment on "A new interpretation of Weimer et al's solar wind propagation delay technique" by Bargatze et al., *J. Geophys. Res.*, *111*, A06102, doi:10.1029/2005JA011376.
Huang, N. E., Z. Shen, S. R. Long, M. L. C. Wu, H. H. Shih, Q. N. Zheng, N. C. Yen, C. C. Tung, and H. H. Liu (1998), The empirical mode decomposition and the Hilbert spectrum for nonlinear and non-stationary time series analysis, *Proc. R. Soc. A*, *454*, 903–995.
Kamide, Y., and S. Kokubun (1996), Two-component auroral electrojet: Importance for substorm studies, *J. Geophys. Res.*, *101*, 13,027–13,046.
Kan, J. R., and L. C. Lee (1979), Energy coupling function and solar wind-magnetosphere dynamo, *Geophys. Res. Lett.*, *6*, 577–580.
Kawasaki, K., and S.-I. Akasofu (1971), Low latitude DS component of geomagnetic storm field, *J. Geophys. Res.*, *76*, 2396–2405.
Klimas, A. J., D. Vassiliadis, N. Baker, and D. A. Roberts (1996), The organized nonlinear dynamics of the magnetosphere, *J. Geophys. Res.*, *101*, 13,089–13,113.
Kovacs, P., V. Carbone, and Z. Voros (2001), Wavelet-based filtering of intermittent events from geomagnetic time-series, *Planet. Space Sci.*, *49*(12), 1219–1231.
Laurenza, M., A. Vecchio, M. Storini, and V. Carbone (2012), Quasi-biennial modulation of galactic cosmic rays, *Astrophys. J.*, *749*, 167.
Lyons, L. R., G. T. Blanchard, J. C. Samson, R. P. Lepping, T. Yamamoto, and T. Moretto (1997), Coordinated observations demonstrating external substorm triggering, *J. Geophys. Res.*, *102*, 27,039–27,051.
Merrill, R. T., M. W. McElhinny, and P. L McFadden (1996), *The Magnetic Fields of the Earth: Paleomagnetism, the Core and the Deep Mantle*, Academic Press, San Diego, Calif.
Newell, P. T., T. Sotirelis, K. Liou, C.-I. Meng, and F. J. Rich (2007), A nearly universal solar wind-magnetosphere coupling function inferred from 10 magnetospheric state variables, *J. Geophys. Res.*, *112*, A01206, doi:10.1029/2006JA012015.
Pallocchia, G., E. Amata, G. Consolini, M. F. Marcucci, and I. Bertello (2007), AE index forecast at different time scales through an ANN algorithm based on L1 IMF and plasma measurements, *J. Atmos. Sol. Terr. Phys.*, *70*, 663–668.
Perreault, P., and S.-I. Akasofu (1978), A study of geomagnetic storms, *Geophys. J. R. Astron. Soc.*, *54*, 547–573.
Rostoker, G., J. A. Vallance, R. L. Gattinger, C. D. Anger, and J. S. Murphree (1987), The development of the substorm expansive phase: The "eye" of the substorm, *Geophys. Res. Lett.*, *14*, 399–405.
Shannon, C. E. (1948), A mathematical theory of communication, *Bell Syst. Tech. J.*, *27*, 379–423.
Sharma, A. S. (1995), Assessing the magnetosphere's nonlinear behavior: Its dimension is low, its predictability, high, *Rev. Geophys.*, *33*, 645–650.
Sitnov, M. I., S. Sharma, K. Papdopoulos, and D. Vassiliadis (2001), Modeling substorm dynamics of the magnetosphere: From self-organization and self-organized criticality to nonequilibrium phase transitions, *Phys. Rev. E*, *65*, 16116.
Sugiura, M., and D. J. Poros (1971), Hourly values of equatorial Dst for years 1957 to 1970, Rep. X-645-71-278, 1971, Goddard Space Flight Cent., Greenbelt, Md.
Tsurutani, B., M. Sugiura, T. Iyemori, B. E. Goldstein, W. D. Gonzalez, S. I. Akasofu, and E. J. Smith (1990), The nonlinear response of AE to the IMF B_s, *Geophys. Res. Lett.*, *17*, 279–282.
Tsurutani, B. T., R. Hajra, E. Echer, and J. W. Gjerloev (2015), Extremely intense (SML ≤ -2500 nT) substorms: Isolated events that are externally triggered?, *Ann. Geophys.*, *33*, 519–524, doi:10.5194/angeo-33-519-2015.
Uritsky, V. M., and M. I. Pudovkin (1998), Low frequency $1/f$-like fluctuations of the AE-index as a possible manifestation of self-organized criticality in the magnetosphere, *Ann. Geophys.*, *16*, 1580–1588.
Uritsky, V. M., A. J. Klimas, D. Vassiliadis, D. Chua, and G. Parks (2002), Scale-free statistics of spatiotemporal auroral emissions as depicted by POLAR UVI images: The dynamics magnetosphere is an avalanching system, *J. Geophys. Res.*, *107*(A12), 1426.
Vassiliadis, D. (2006), System theory for geospace plasma dynamics, *Rev. Geophys.*, *44*, RG2002, doi:10.1029/2004RG000161.
Vecchio, A., M. Laurenza, V. Carbone, and M. Storini (2010a), Quasi-biennal modulation of solar neutrino flux and galactic cosmic rays by solar cyclic activity, *Astrophys. J. Lett.*, *709*, L1–L5.
Vecchio, A., V. Capparelli, and V Carbone (2010b), The complex dynamics of the seasonal component of USA's surface temperature, *Atmos. Chem. Phys.*, *10*, 9657–9665.
Vecchio, A., M. Anzidei, V. Capparelli, V. Carbone, and I. Guerra (2012a), Has the Mediterranean Sea felt the March 11th, 2011, M_w 9.0 Tohoku-Oki earthquake?, *Europhys. Lett.*, *98*, 59001.
Vecchio, A., M. Laurenza, D. Meduri, V. Carbone, and M. Storini (2012b), The dynamics of the solar magnetic field: Polarity reversals, butterfly diagram, and quasi-biennial oscillations, *Astrophys. J.*, *749*, 27.
Vecchio, A., F. Lepreti, M. Laurenza, T. Alberti, and V. Carbone (2017), Connection between solar activity cycles and grand minima generation, *Astron. Astrophys.*, *599*, A58, doi:10.1051/0004-6361/201629758.
Wanliss, J. A. (2005), Fractal properties of SYM-H during quiet and active times, *J. Geophys. Res.*, *110*, A03202, doi:10.1029/2004JA010544.
Wanliss, J. A., and V. Uritsky (2010), Understanding bursty behavior in midlatitude geomagnetic activity, *J. Geophys. Res.*, *115*, L04107, doi:10.1029/2009JA014642.
Weimer, D. R., and J. H. King (2008), Improved calculations of interplanetary magnetic field phase front angles and propagation time delays, *J. Geophys. Res.*, *113*, A01105, doi:10.1029/2007JA012452.
Weimer, D. R., D. M. Ober, N. C. Maynard, M. R. Collier, D. J. McComas, N. F. Ness, C. W. Smith, and J. Watermann (2003), Predicting interplanetary magnetic field (IMF) propagation delay times using the minimum variance delay technique, *J. Geophys. Res.*, *108*(A1), 1026, doi:10.1029/2002JA009405.
Wu, Z., and N. E. Huang (2004), A study of the characteristics of white noise using the empirical mode decomposition method, *Proc. R. Soc. A*, *460*, 1597–1611.